12 Corrosion in Molten Salts

K. Sridharan, T.R. Allen

Department of Engineering Physics, University of Wisconsin–Madison, Madison, Wisconsin

12.1 Introduction

Molten salts have many industrial uses, such as electrolytes for fuel cells and molten metal batteries, heat treatment of industrial components, pyroprocessing for extraction and purification of metals, heat transfer and storage, coal gasification, and destruction of chemical weapons. Molten salts have been considered for multiple applications within nuclear energy systems, such as primary and secondary coolants in fission and fusion systems, media for advanced electrochemical recycling of used fuel, and zirconium purification [1,2].

The applications for molten salts can be generically divided into two categories: primary salts, those used to directly cool the fuel that produces heat through nuclear fission, and secondary salts that transfer high temperature process heat from the primary system for applications, such as electricity and hydrogen production and operation of chemical industry and desalination plants. An extensive review of thermal, thermophysical, and nuclear properties and costs of various salts and salt combinations for nuclear fission applications has been performed [3]. For nuclear fission applications, a salt requires chemical stability, low volatility, a low melting point, and a high boiling point. Additionally, the salts must be compatible with the combinations of structural materials used in the nuclear systems, which can range from various alloys to graphite and composites. For applications in the primary reactor circuit, the salt must have a low neutron capture cross section to maximize fuel utilization, be stable under intense radiation, and have good fission product retention characteristics. Since large quantities of salts will be required in potential nuclear energy systems, relative costs of salts will be an important consideration.

Using the aforementioned criteria, salts for primary coolants fall into three categories [3]: (i) alkali fluorides, (ii) mixtures of alkali fluorides and BeF_2, and (iii) mixtures of alkali fluorides and ZrF_4. Four alkali fluorides, four mixtures of alkali fluorides and BeF_2, and seven mixtures of alkali fluorides and ZrF_4 have been highlighted for consideration as primary coolants. For secondary coolants, fluoride, fluoroborate, and chloride salts have been identified as possible candidates with two fluoride salts, three fluoroborate salts, and seven chloride salts specifically warranting consideration.

The foundational work for the use of molten salts in nuclear energy applications was performed at the Oak Ridge National Laboratory (ORNL) in the United States in the 1940s through the 1970s, first in the Aircraft Reactor Experiment (ARE) and subsequently in the larger Molten Salt Reactor Experiment (MSRE). Research findings from these experiments have been documented extensively in original ORNL technical reports and papers [4–18]. These experiments resulted in nuclear reactors with uranium fuel (as fluoride)

dissolved in molten fluoride salts. The ARE led to the development of a high power density reactor that used 53.09% NaF–40.73% ZrF_4–6.18% UF_4 (mol%) molten salt and operated at a maximum power of 2.5 MW. The MSRE led to the development of a civilian graphite-moderated 7.5 MW breeder reactor that used 64% LiF–30% BeF_2–5% ZrF_4–1% UF_4 (mol%) molten salt operated at 650 °C [4,5]. This salt was made up of low neutron cross-section elements to achieve the highest possible breeding ratio and the LiF component used enriched ^{7}Li for better neutron economy. The molten salt fast spectrum reactor program at CSNR in France is considering a LiF-ThF_4-UF_4 salt [1]. Both the early ORNL reactors and the CSNR reactor are based on a homogeneous fluid fuel, with the uranium fuel dissolved in the molten salt. The molten LiF-BeF_2 (FliBe) salt is the leading primary candidate for coolants in nuclear fusion power systems.

In recent reactor design programs for salt-cooled reactors, where salt cools the fuel but the fuel is not dissolved in the salt [known alternatively as advanced high temperature reactors (AHTR) or fluoride-cooled high temperature reactors (FHR)], the principal choice for the primary coolant salt is FLiBe prepared again with enriched ^{7}Li to minimize the loss of fission neutrons to the salt [19–21]. These reactor concepts will use TRISO (TRistructural ISOtropic) fuel particles (similar to those developed for the high temperature gas-cooled reactor, HTGR) immersed in the primary coolant salt.

Molten LiCl-KCl eutectic composition salt has been used as the medium for electrochemical recycling (pyroprocessing) of used nuclear fuel [22,23]. More recently, the attractive thermophysical properties of molten salts have also led to their consideration as heat transfer media for intermediate loops for the transfer of high-temperature process heat from AHTR and HTGR to power chemical industries and desalination plants [24,25]. Some salts such as fluoride salt 46.5% LiF–11.5% NaF–42% KF (in mol%, known as FLiNaK) and a chloride salt 68% KCl–32% $MgCl_2$ (mol%) are being investigated for this application [26]. Finally, fluoroborate, mixed halide, and nitrate salts have received consideration for secondary coolants for tritium extraction [3,5,6]. A limitation of nitrate salts is their relatively low decomposition temperature (≈600 °C). The rest of the chapter focuses mainly on corrosion in molten fluorides and, to some extent, on molten chloride and fluoroborate salts because of their wide-spread significance in nuclear energy systems; however, the concepts discussed are readily applicable to other types of salts as well.

12.2 Corrosion in Molten Fluoride Salts

In most high-temperature environments, corrosion resistance in materials is achieved by the formation of a tenacious and protective oxide film on the alloy surface [27]. For example, for high-temperature applications in oxygen-containing environments, alloys containing elements such as Cr, Al, and Si are used routinely to promote the formation of self-healing protective surface oxide films that act as diffusion barriers and reduce the rate of further oxidation. However, in fluoride salt systems, any such protective oxide films dissolve by the fluxing action of molten fluoride salts and cannot be relied upon for corrosion protection [5,6,28–32]. Once the passive oxide film is removed, corrosion proceeds by the attack of the least noble constituent of the freshly exposed alloy surface. Corrosion is then driven by a variety of factors, including thermodynamics of corrosion reactions, impurity effects, and activity and temperature gradients.

12.2.1 Thermodynamic Considerations

The difference in the free energy of the salt fluoride constituents and the fluorides of the alloying elements is a key driving force for corrosion [29–36]. Thus, metals that have high negative free energies of fluoride formation are generally more prone to corrosion, that is,

they are more likely to form a fluoride compound and dissolve in the salt. For a basic fluorination reaction of a solid metal M,

$$x\mathrm{M(solid)} + y\mathrm{F_2(gas)} = \mathrm{M}_x\mathrm{F}_2y\mathrm{(liquid)} \tag{12.1}$$

The Gibbs free energy of formation of a fluoride compound (per mole of the fluoride compound) can be calculated by subtracting the Gibbs free energy of the reactant phases from those of the products phases. The Gibbs free energies of the formation of select fluoride compounds are listed in Table 12.1 [29,33,34].

Table 12.1 shows, for example, that the thermodynamic free energies of the formation of alkali and alkaline earth metals that make up the salts such as FLiNaK and FLiBe are more negative than the common components of structural alloys, with Cr being most prone to attack. Thus, in pure salts with no impurities, structural alloys should be in equilibrium with the salt melt and, once at equilibrium, not corrode further based on thermodynamic considerations. Note that the highly corrosive hydrofluoric acid (HF) has a reasonably high negative free energy of formation. HF can form through reaction with moisture or other impurities and lead to a severe corrosion of containment systems as discussed in the subsequent sections.

Work at NASA on the corrosion of a wide range of structural alloys in FLiNaK and other fluoride salts presents thermodynamic calculations to define equilibrium conditions for possible corrosion reactions [37,38]. Although these studies were performed for thermal storage systems, they do shed light on some features of corrosion in molten fluoride salts in general. For closed systems, the equilibrium concentration of the corrosion product fluorides in the salt melt dictates the maximum extent of corrosion and would be important in the long-term corrosion of containment materials. The corrosion of a pure metal M (Ni, Co, Fe, or Cr) in an alkali fluoride, i.e., Me-fluoride (Me being, for example, Li, Na, K) is given by

$$x\mathrm{M} + y\mathrm{MeF} = \mathrm{M}_x\mathrm{F}_y + y\mathrm{Me} \tag{12.2}$$

For Ni, Co, Fe, and Cr, the $\mathrm{M}_x\mathrm{F}_y$ compound would be NiF_2, CoF_2, FeF_2, and CrF_2/CrF_3. However, for Al, heat of mixing data suggests that a complex species AlF_6^{+3} may form, resulting in the reaction,

$$6\mathrm{MeF} + \mathrm{Al} = \mathrm{Me_3AlF_6} + 3\mathrm{Me} \tag{12.3}$$

Table 12.1 Free Energy of Formation of Common Fluoride Compounds of Constituents of Salt and Structural Materials at 727 °C, Unless Specified [29,33,34]

Fluoride Compound	Free Energy of Formation (Kcal/mol-F)	Fluoride Compound	Free Energy of Formation (Kcal/mol-F)
LiF	−125	AlF_3	−90
MgF_2	−113	CrF_2	−75.2
NaF	−112	CrF_3	−72.3
Rb	−112	FeF_2	−66.5
KF	−109	FeF_3	−60.6 (at 754 °C)
BeF_2	−104	WF_6	−56.8
ZrF_4	−94	NiF_2	−55.3
HF	−66.2	MoF3	−52.5 (at 754 °C)

The equilibrium concentration of M_xF_y and Me_3AlF_6 in the molten salt would determine the maximum extent of corrosion. Based on this, the equilibrium concentration of corrosion product fluorides (Ni, Fe, Co, Cr, and Al) in the three individual alkali salts constituting FLiNaK, namely, LiF, KF, and NaF at 827°C, has been calculated assuming ideal solution behavior. Based on this analysis, the tendency for common alloying constituents to be attacked in molten fluoride salts increases in the following order: Ni, Co, Fe, Cr, and Al, with Al being the most prone to dissolution. Most structural alloys investigated in this NASA study did not contain Al and the depth of attack correlated with the Cr content of the alloys. Attack occurred predominantly along the grain boundaries. Selective attack of Cr in fluoride salts has been observed in numerous studies [6–10,29,30]. A multicomponent alloy will be corroded by the oxidation and removal of the least noble component. It has been shown that the solubility of alloy metal fluorides is lower for LiF salt compared to NaK and KF salt; consequently, the latter two salts would be more corrosive. Again, these calculations assume an ideal solution, that is, the activity of M_xF_y in the melt is considered to be unity. This is a critical assumption, especially for salt mixtures that exhibit large deviations from ideal thermodynamic behavior. Another observation in these NASA studies is the importance of container material in which the corrosion tests were performed. For most materials tested, corrosion observed for materials in a quartz container was higher compared to an alumina container. A possible reason for this is that SiO_2 from quartz participates in the reaction with water and NaF to release HF gas and enhance corrosion [38]. The importance of container material on the corrosion behavior of test materials has been observed in other studies and is discussed in later sections.

Another important aspect of understanding corrosion in molten fluoride salts is the Lewis acid–base properties of the salt [5,29,35]. A Lewis acid is defined as an electron pair acceptor, and a Lewis base as an electron pair donor. Salts such as ZrF_4 and BeF_2 would be examples of Lewis acid and could react with fluoride ions from basic salts (e.g., alkali fluoride salts) to form complexes as, for example,

$$ZrF_4 + 2F^- \rightarrow ZrF_6^{2-} \tag{12.4}$$

$$BeF_2 + 2F^- \rightarrow BeF_4^{2-} \tag{12.5}$$

Thus, if an acidic salt, BeF_2, was to be added to LiF, a basic salt, it would tend to form a complex BeF_4^{2-} ion. The result of such a complexation is stabilization of the acid component and a decrease in its chemical activity. In effect, complexation immobilizes and ties up the F^- ions coming from the basic salt [35]. It influences many of the properties of the salt, but its effect on activity coefficients is particularly relevant to understanding corrosion in molten salts. This can, for example, explain the higher corrosion observed in alkali metal salts (basic salt) compared to NaF-ZrF_4-UF_4 (acidic salt). The lower corrosion observed in acidic salt is related to the stability of the corrosion product by complexation with the higher activity of fluoride ions in the basic salt mixture [5,35].

12.2.2 Impurity-Driven Corrosion

One of the most significant concerns in molten salt systems is corrosion driven by the impurities present in the salt. Impurities such as moisture, hydroxides, and oxides from the environment, as well as metallic impurities from containment systems, can get incorporated in the salt during manufacture and storage of the salt. The inherently hygroscopic nature of these salts exacerbates this problem. The importance of impurity-driven corrosion was

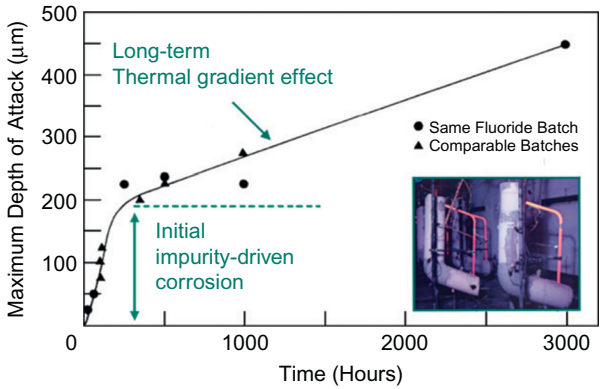

Figure 12.1 Depth of corrosion attack in Inconel 600 in molten fluoride salt as a function of exposure time. (Inset) Photograph of the loop in which the tests were performed [31].

recognized and documented extensively in the ORNL work and corroborated by subsequent researchers [5,6,9,17,31–38]. Figure 12.1 shows the characteristic pattern observed in these experiments, carried out in closed convection loops [31].

Impurities drive corrosion at a rapid rate in the early stages of the process, but the later stages of corrosion are driven by thermal gradient and other effects (discussed later). Once the impurities are exhausted, corrosion exhibits a slower linear relationship with time. These studies indicate the importance of on-line control of salt purity and chemistry in molten salt systems. The variations in corrosion rate data observed in the molten salt research literature may in part be attributable to the levels of impurities in salts used, even though the nominal compositions may be identical. The impurity-driven effects may also be responsible for discrepancies in corrosion data taken from short-term tests (when the impurity effect is still dominant) compared to those taken from long-term tests. Accurate analysis of trace quantities of impurities, particularly corrosive anionic impurities, continues to be a challenge, placing a high premium on salt manufacture and purification steps prior to use. For the same reason, corrosion experiments (including salt handling) must be conducted in atmosphere-controlled enclosures. In addition to impurities in the salts, oxide films on container walls can also accelerate corrosion and must be cleaned or flushed with salt prior to use. Moisture is perhaps the most deleterious contaminant in molten fluoride salts because it can react with salt fluorides (MeF) to form the highly corrosive hydrofluoric acid according to the following reactions [29]:

$$\mathrm{MeF(l) + H_2O(g) = MeOH(l) + HF(g)} \tag{12.6}$$

$$\mathrm{2MeF(l) + H_2O(l) = Me_2O(l) + 2HF(g)} \tag{12.7}$$

H_2 can then be formed by the reaction of water or hydrofluoric acid with the constituents of alloys (M), and any oxide of salt constituents (Me) can be fluxed by hydrofluoric acid via the following reactions [37,38]:

$$x\mathrm{M} + y\mathrm{H_2O} = \mathrm{M}_x\mathrm{O}_y + y\mathrm{H_2} \tag{12.8}$$

$$x\mathrm{M} + y\mathrm{HF} = \mathrm{M}_x\mathrm{F}_y + \frac{y}{2}\mathrm{H_2} \tag{12.9}$$

$$\mathrm{Me_2O + 2HF = 2MeF + H_2O} \tag{12.10}$$

These reactions will lead to the accumulation of oxides and fluorides (and even hydroxides) of the alloy constituents. Furthermore, water can react with alloying constituents to form oxides and fluorides, which can dissolve into the salt.

Metallic impurities in the salt such as Fe and Ni incorporated as fluorides in the salt during its manufacture can react with Cr in the alloy (most high temperature structural alloys contain Cr for air-side oxidation resistance) and result in the following corrosion reactions [9]:

$$NiF_2 + Cr = CrF_2 + Ni \tag{12.11}$$

$$FeF_2 + Cr = CrF_2 + Fe \tag{12.12}$$

$$2HF + Cr = CrF_2 + H_2 \tag{12.13}$$

$$6HF + 2Cr = 2CrF_3 + 3H_2 \tag{12.14}$$

These reactions effectively leach Cr out the alloy into the salt. In fact, intentional additions of FeF_2 to the molten salt during experiments have been shown to enhance corrosion [17].

Oxides on the surface of the alloy can lead to corrosion by constituents in the salt,

$$2NiO + ZrF_4 = ZrO_2 + 2NiF_2 \tag{12.15}$$

Finally, direct reduction of UF_4 (in fuel containing salts) by Cr in the alloy can also corrode and leach Cr from the alloy,

$$2UF_4 + Cr = CrF_2 + 2UF_3 \tag{12.16}$$

In the particular case of FLiBe salt, moisture can lead to the formation of oxide phases and HF [34],

$$BeF_2 + H_2O = BeO + 2HF \tag{12.17}$$

$$2LiF + H_2O = Li_2O + 2HF \tag{12.18}$$

$$2HF + Cr = CrF_2 + H_2 \tag{12.19}$$

Figure 12.2 shows cross-sectional photomicrographs of the Inconel 600 alloy after exposure to fuel containing fluoride salt and depicts the role of impurities in corrosion [31]. The microstructure of the corroded depth is typical of corrosion damage observed for alloys tested in molten fluoride flow loops. It consists of uniformly distributed voids that extend well into the subsurface regions of the material. It has been proposed that as chromium diffuses out into the salt, chromium from the interior of the alloy diffuses down the concentration gradient to the surface. Since substitutional diffusion occurs by a vacancy migration process, an excess of vacancies can build up in the metal, which can coalesce to form voids [17].

It is clear from the aforementioned example reactions that impurities in the salt must be strictly controlled in order to mitigate corrosion. Recognizing this issue, extensive purification protocols were instituted in the ORNL experiments and further improved by other

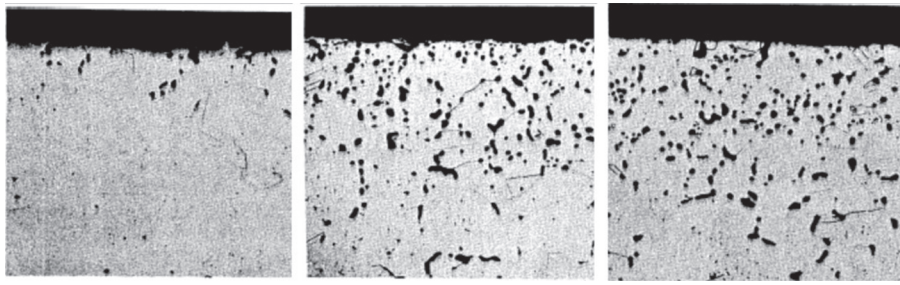

Figure 12.2 Cross-sectional images of Inoconel 600 alloy after corrosion tests in fuel-containing molten fluoride salt containing (a) low Fe and Ni, (b) high Fe and Ni, and (c) high HF [31].

researchers [34,36]. The first step is typically a vacuum-drying process ($\approx 10^{-3}$ mm Hg) to remove moisture. The next step is a hydrofluorination treatment, which involves sparging the molten salt with the H_2/HF mixture for up to 20 h to remove the moisture/oxide impurities from salts such as FLiNaK and FLiBe [28,32,34,36]. This treatment also removes other corrosive impurity species such as halide and sulfur (removed as acids or H_2S gases). This may be followed by treating the salt melt with an active metal such as Zr or Be to reduce the oxidation potential of the salt. This active metal treatment removes impurities such as HF, moisture, and hydroxides but it does not affect the removal of halide and sulfur contaminants. A number of other purification steps have been recommended, but this would depend on the nature of the application [34,36]. For example, a less rigorous purification method may be required for coolant salts than those used for fuel-bearing salts toward which much of the purification research at ORNL was oriented. Once the impurities are removed, the salts should be kept away from the atmosphere and moisture to maintain their purity.

12.2.3 Thermal Gradient-Driven Corrosion

The solubility of fluoride corrosion products in molten salts is a strong function of temperature. Thus the products of corrosion dissolved at the higher temperature sections of the system can partially plate out in the relatively cooler sections of the system. The driving force for this mass transport of the corrosion product is the difference in temperature between the hot and the cold sections. The cooler side in effect becomes a sink for the corrosion product continually depleting the molten salt of the corrosion product, thereby facilitating more corrosion on the hotter side [30]. A physical mechanism for this type of corrosion has been proposed wherein leaching of the alloy constituent on the hot side increases to a point where its concentration on the cooler side reaches its saturation limit in the salt, leading to its nucleation as a solid on the metallic wall of the cooler section and building up as a plating and even diffusing into the surface [17]. This phenomenon is particularly important in coolant salts where the corrosion products from the primary circuit (hotter sections) can deposit on the relatively cooler heat exchanger to the secondary circuit and can potentially lead to the clogging of components such as heat exchangers. Investigation of thermal gradient-driven corrosion has been studied extensively in natural convection or forced convection loops [5,6,17,30]. The loops typically consist of a hot section and a relatively cooler section (Figure 12.3). In the MSRE program, when investigating the long-term corrosion

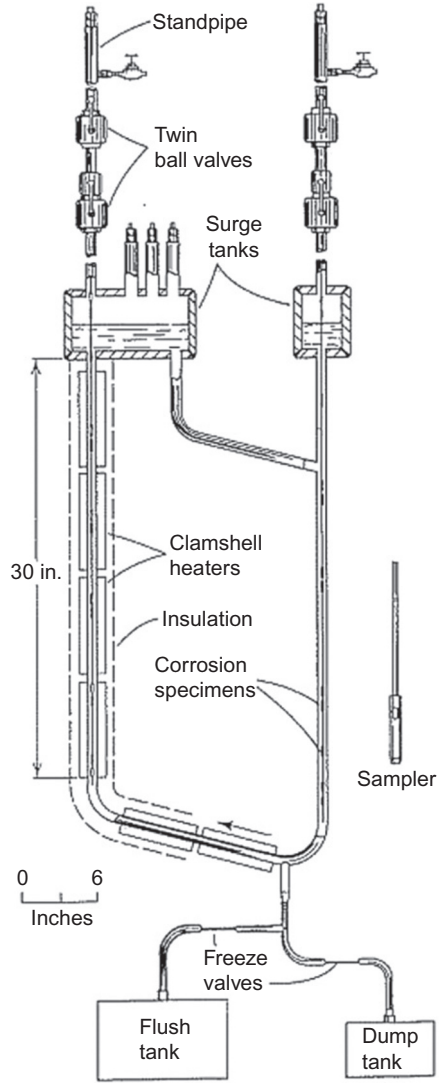

Figure 12.3 Typical molten salt convection flow loop showing hot sections (with heaters and insulation) and cooler section [30].

performance of Hastelloy N, the hot section of the loop (also made of Hastelloy N) was maintained at 700 °C, while the cooler section of loop was maintained at 560 °C. After 9 years of testing, Hastelloy N on the hotter side had developed severe voids up to depths of 50 μm, while the cooler side exhibited deposition of material [18]. Typical data from loop studies are shown in Figure 12.4, where with exposure time the samples on the hot side lost mass while the samples on the cooler side correspondingly gain mass. These loop experiments allow for the study of corrosion that include the effects of thermal gradient, flow, chemistry changes, and surface area effects [30].

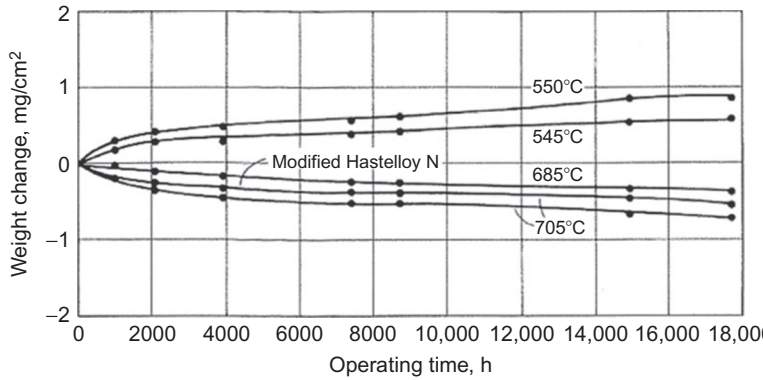

Figure 12.4 Weight changes on hot and cold sections of the flow loop with exposure time for Hastelloy N samples exposed to LiF-BeF_2-ThF_4-UF_4 molten salt [18,30].

12.2.4 Dissimilar Material Corrosion

The presence of dissimilar materials in the vicinity of each other in molten salts can provide the driving force and, in fact, accelerate corrosion. The dissolved species from the material with higher activity can migrate and deposit on the second material with a lower activity of the dissolved species. For example, the deposition of cobalt has been documented on Hastelloy N (0.1% Co) from Co-rich Alloy-25 (53% Co) when the two alloys were placed in the vicinity of each other in a molten salt medium [39]. Corrosion driven by activity gradients can be particularly pronounced if the second material has a chemical affinity for the dissolved species and forms thermodynamically favorable compounds. Activity-driven corrosion becomes a particular issue in static corrosion studies where the crucible containment material has been noted to have a significant effect on the corrosion of test materials, and also when multiple diverse materials are in proximity to each other in a molten salt.

A detailed study was undertaken to evaluate the corrosion performance of a wide range of candidate high-temperature structural alloys in molten FLiNaK salt (at 850 °C for 500 h exposure) for secondary heat transfer applications [29,40,41]. The study is illustrative of both the relative performances of the alloys tested in this fluoride salt and the significance of dissimilar materials corrosion. Alloys tested in this study included Hastelloy N, Hastelloy X, Inconel 617, Incooly 800H, Haynes 230, and Ni-201, a nearly pure Ni alloy. Severe corrosion was observed in all the alloys (with the exception of Ni-201), with the graphite container material (including graphite fixturing rods) becoming cathodic with respect to the test materials and accelerating corrosion significantly. A depletion of Cr was observed at the surface of the alloys in both grains and grain boundaries with the attack being markedly severe along the grain boundaries. Figure 12.5 shows the weight loss for the various alloys after corrosion tests. For Hastelloy N, Mo-rich precipitates were still observed to be intact at the grain boundaries due to the relatively low negative free energy of formation of molybdenum–fluoride. The severity of the corrosion attack correlated reasonably well with the chromium content of the alloy, except for alloys containing alloys 20 to 23% Cr content (Figure 12.6a). However, as shown in Figure 12.6b, for these high chromium alloys there appears to be a more direct correlation between the carbon content of the alloy and the chromium content in the salt after the corrosion tests [41]. This indicates that a connective structure of Cr-carbides at the surface and pronounced grain boundary attack appear to be correlated. Figure 12.7 shows cross-sectional scanning electron microscopy (SEM) images

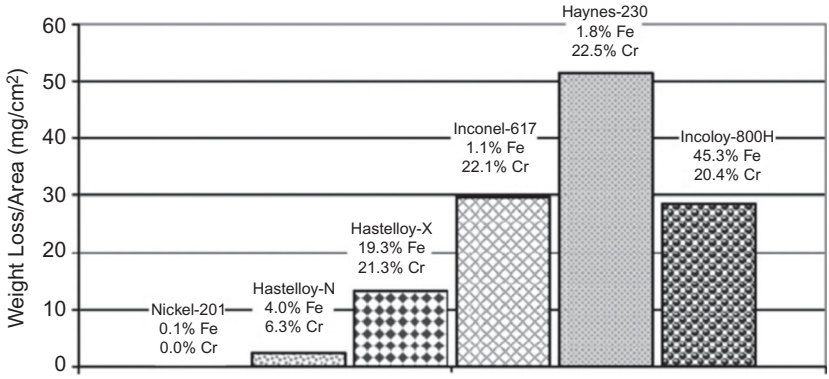

Figure 12.5 Weight loss measurements of various alloys after corrosion testing in molten FLiNaK salt at 850 °C for 500 h. Tests were conducted in graphite container.

Figure 12.6 (a) Correlation between chromium content in the alloys and weight loss due to corrosion and (b) correlation between carbon content of the high chromium alloys and weight loss in the alloys due to corrosion. Tests were conducted in graphite crucibles [41,42].

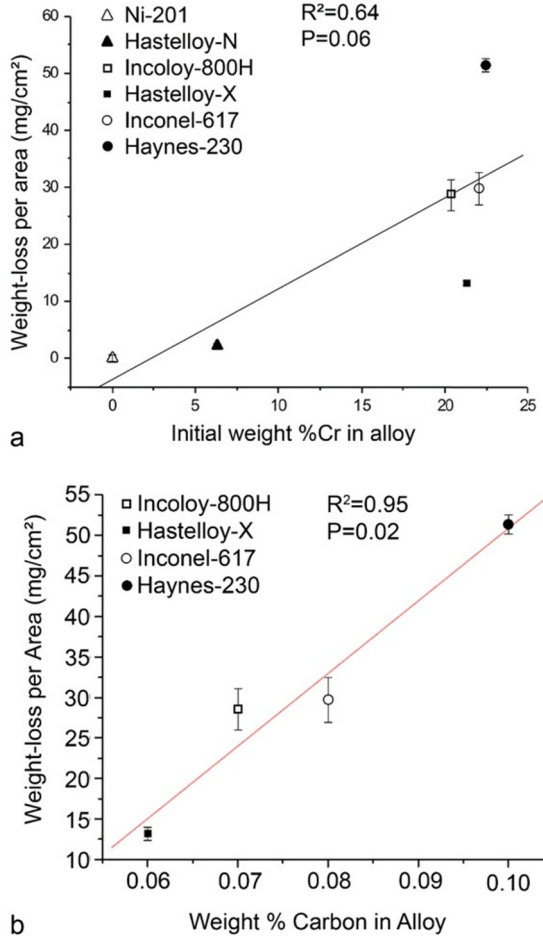

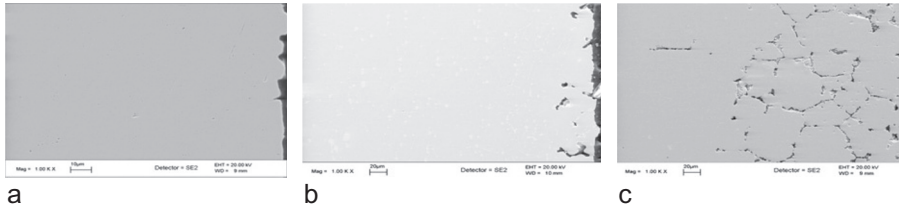

Figure 12.7 Cross-sectional SEM image of the surface of alloys after corrosion testing in molten FLiNaK salt at 850 °C for 500 h: (a) Ni-201 (no Cr), (b) Hastelloy N (6.3% Cr), and (c) Hastelloy X (21.3% Cr). Tests were conducted in graphite container [29].

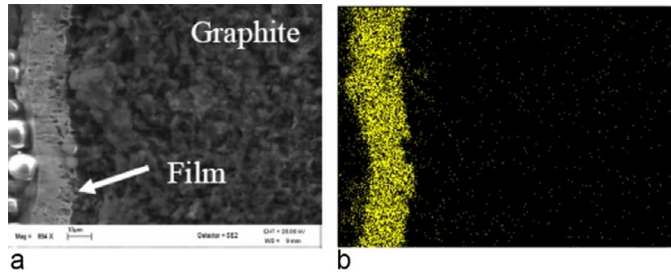

Figure 12.8 (a) Cross-sectional SEM image of graphite central fixturing rod after corrosion tests with Incoloy 800H showing corrosion film formation, ≈15-μm thick carbide layer and (b) EDS X-ray elemental mapping of confirming the film to be largely composed of a Cr-rich phase [29].

of some of the materials after the corrosion tests that confirm the important role of chromium in corrosion in the molten fluoride salt FLiNaK.

An examination of the graphite crucibles and sample fixturing rods after corrosion tests clearly showed the formation of Cr-carbide on the graphite surface [29]. Chromium from the alloy dissolved into the salt (possibly due to impurity-driven corrosion), migrated to the graphite, and formed Cr_7C_3 Cr-carbide on the surface of graphite as confirmed by SEM-energy dispersive spectrometer (EDS) analysis, X-ray photoelectron spectroscopy, and X-ray diffraction techniques. Figure 12.8 shows the formation of Cr-carbide on the graphite fixturing rods.

Subsequent tests performed using the same material containers as the test alloys confirmed that this acceleration effect was due to dissimilar materials, but also showed that the basic mechanisms of corrosion in the material did not change significantly as a result of using the graphite containers [29]. The weight change measurements of Incoloy 800H samples tested in graphite crucibles with those performed in Incoloy 800H are shown in Figure 12.9. The weight loss measured from the Incoloy 800H samples in the Incoloy 800H containers was miniscule in comparison to those with tests performed in graphite capsules. This difference in weight loss highlights the increase in corrosion of the alloy test samples due to graphite promoting chromium dealloying from the alloy into the salt. The chromium content of the salt determined by neutron activation analysis after the graphite container test was 372 ± 21 ppm Cr compared to 99.8 ± 5.1 ppm Cr in the Incoloy-800H container tests.

While shedding light on the relative corrosion performance of alloys, these studies also illustrate the effect of dissimilar metals on corrosion in molten salts. This should be differentiated from situations where the container material reacts with the salt and alters the corrosion rate of test materials, as was observed in NASA studies performed in quartz crucible materials [37,38].

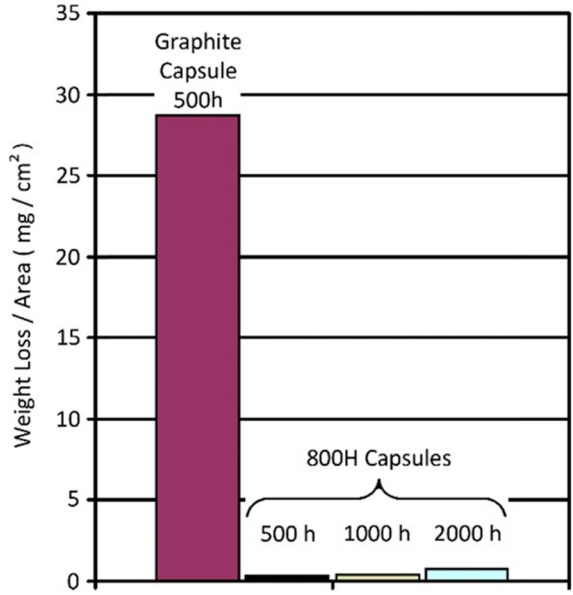

Figure 12.9 Comparison of weight loss due to corrosion in FLiNaK at 850 °C for 500 h for Incoloy-800H samples tested in graphite and Incoloy-800H containers [29].

12.2.5 Redox Control and Electrochemistry

The corrosivity of molten salts due to the various factors discussed earlier, particularly by the presence of impurities, may require that the oxidation potential of the salt be lowered by the addition of elements or compounds to mitigate corrosion. The redox potential of a salt mixture is its effective potential for oxidation or reduction of the cations that make up the salt [28,29]. The redox potential is related directly to the oxidation states of the metal ions in the molten salt mixture that are capable of having multiple oxidation states [5,28]. For the constituents of the salts investigated in the ORNL experiments, LiF, NaF, KF, BeF_2, and ThF_4 have neither higher nor lower valence states [5]. However, uranium that was added to the salt has multiple valence states, namely, UF_3, UF_4, UF_5, and UF_6. Higher valence states are more corrosive, as they can potentially undergo multiple reductions. This fact was utilized effectively in the MSRE experiments to control corrosion. For example, in the fuel-bearing salts used in this study, UF_4 reacted with Cr in the structural material and promoted its dissolution into the salt according to the reaction

$$Cr + 2UF_4 = 2UF_3 + CrF_2 \tag{12.20}$$

The corrosion here was controlled by the addition of small amounts of UF_3 to maintain a UF_3/UF_4 ratio greater than 0.005. This shifted Reaction (12.20) to the left and effectively suppressed corrosion. A very high UF_3/UF_4 would make the salt less corrosive; however, it would also make the salts highly reducing, raising concerns of reduction to metallic uranium or formation of uranium carbide in the presence of graphite [5]. The upper limit for this ratio was decided to be 0.06 in the MSRE studies.

The thermodynamic free energies (ΔG) can be converted to electromotive force scale (E) using the expression

$$E_0 = \frac{\Delta G_0}{n\mathrm{F}} \tag{12.21}$$

where n is the valence and F is the Faraday constant.
The redox potential (e_M) of a salt melt is determined by the Nernst equation [42,43].

$$M^{2+} + 2e = M \tag{12.22}$$

$$e_M = e^{\circ}{}_M + 2.3\frac{RT}{2F}\log\left(\frac{[M^{+2}]}{[M]}\right) \tag{12.23}$$

The redox potential can be measured experimentally using electrochemistry techniques. Lower redox potentials lower corrosion. As discussed in a later section, control of the redox potential of the molten fluoride fuel salt also reduced fission product tellurium-induced stress corrosion cracking in Hastelloy N.

Beryllium added to FLiBe salt has been shown to reduce corrosion. An example of this is shown in Figure 12.10 where the corrosion of 316 stainless steel was evaluated in LiF-BeF_2 FLiBe salt in a convection loop with a maximum temperature of 650 °C [6]. Note that in the initial stages (up to about 2000 h) the corrosion of 316 stainless steel (as manifested by weight loss) is quite rapid due to impurity-driven effects following which the corrosion rate decreases. Based on corrosion observed between 3000 and 9000 h, a corrosion rate of 8 μm/year was estimated in this study. The addition of beryllium reduced the oxidation potential of the salt and drastically reduced the corrosion rate to an estimated value of 2 μm/year. This result is particularly significant because improvement from the beryllium addition was observed in the initial impurity-driven corrosion regime. In these experiments, the oxidation potential was monitored by on-line voltammetry. That said, continuous control of the redox potential by reducing agents in large molten salt systems can be quite challenging [35]. Additions of rare earths (Sm and Y) and vanadium redox buffers Sm^{+3}/Sm^{+2} and Yb^{+3}/Y^{+2} and V^{+3}/V^{+2} have been suggested for corrosion control in nonfuel bearing salts such as FLiBe, which is being proposed as a primary coolant for the FHR [44].

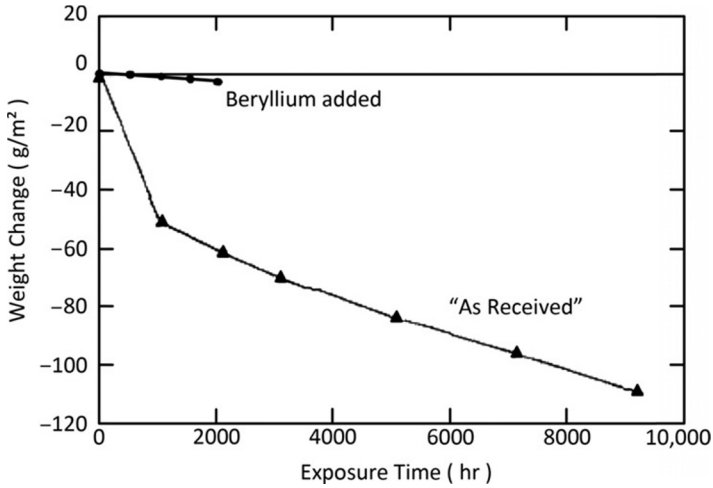

Figure 12.10 Weight-loss 316 stainless steel in the hot section of the loop at 650 °C in LiF-BeF_2 molten salt showing the effectiveness of beryllium additions in controlling the oxidation potential of the salt [6].

The effectiveness of various approaches to control corrosion in fluoride salts has been evaluated based on fluorine potential as the redox condition as defined for the reaction [45]:

$$MF_n + {}^1/_2F_2(g) = MF_{n+1} \tag{12.24}$$

$$\Delta G = RT \ln p_{F2} \tag{12.25}$$

Based on this, the efficacy of providing redox conditions was evaluated in this study for the following approaches: (i) gas phase control by introduction of the H_2/HF redox couple, (ii) Be addition Be/BeF_2 redox couple, (iii) Li addition Li/LiF redox couple, and (iv) addition of cerium–fluoride CeF_3/CeF_4 redox couple. The fluorine potential was calculated from the Gibbs energy of the reaction, which was determined to be −141, −215.7, −253.4, and −18 kcal/mol for H_2/HF, Be/BeF_2, Li/LiF, and CeF_3/CeF_4 redox couples, respectively. According to this study, the Li/LiF redox couple, while being the most desirable, would introduce the possibility of reduction of BeF_4. The Be/BeF_2 redox couple would be applicable to FLiBe, but due to low solubilities, it may be difficult to sustain the redox conditions. To ensure that reducing conditions prevail over the entire loop, a combination of additions of Be and adjustments in the CeF_3/CeF_4 ratio is recommended [45].

On-line electrochemistry can also be used to measure and monitor the concentration of a corroding species such as chromium in the salt, thereby providing an *in situ* assessment of the corrosion of construction components. The anodic stripping voltammetry technique has been used for this purpose, where the integrated current due to oxidation of the corroding species (i.e., Cr) is related to the concentration of the species [46]. Using molten salt with known but varying concentrations of chromium and measuring the integrated current for each concentration, a working curve of concentration and integrated current is determined (Figure 12.11). Such a working curve would allow for the determination of unknown chromium concentrations in the molten salt.

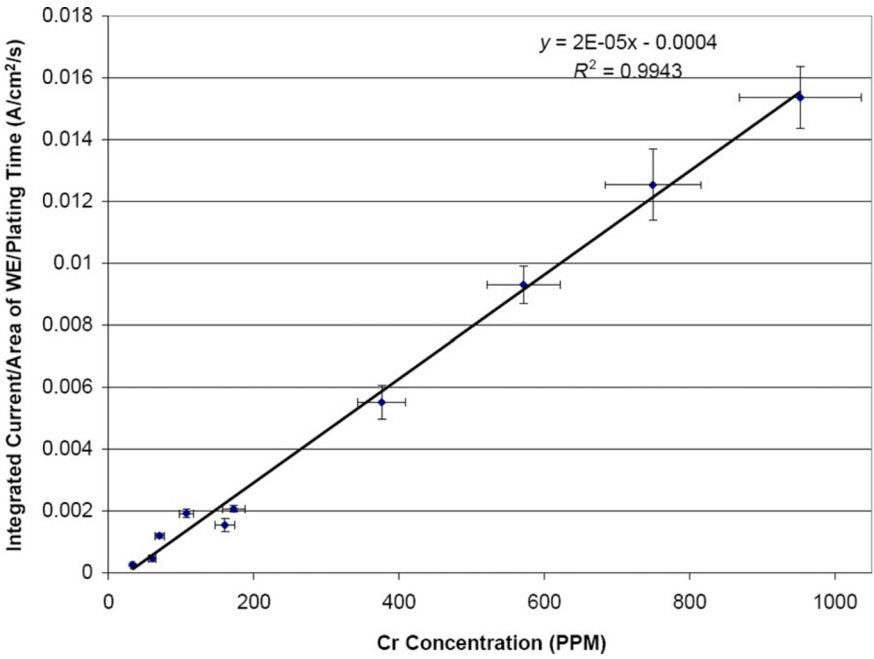

Figure 12.11 Working curve for concentrations of Cr in molten FLiNaK salt at 650 °C as a function of integrated current [46].

12.2.6 Materials Development and Performance in Molten Fluoride Salts

Development of Hastelloy N during the MSRE project marked a significant step toward achieving corrosion-resistant structural materials in a molten fluoride salt environment [4–8,10,18,36,39]. This alloy was developed specifically as container material for the molten salt reactor for sustained corrosion resistance in the fuel-bearing molten fluoride salt 64% LiF–30% BeF_2–5% ZrF_4–1% UF_4 (mol%).

The preceding ARE program used Inconel 600 (78% Ni–15% Cr–7% Fe) as the container material in 53.09% NaF–40.73% ZrF_4–6.18% UF_4 (in mol%). This alloy was suitable for short-term exposures; however, post-test examination indicated unacceptable levels of corrosion at 700 °C, and the alloy was deemed unsuitable for long-term corrosion resistance. Given the propensity of chromium to oxidize and leach into molten fluoride salts and the low negative free energy of the formation of Ni and Mo fluorides, an extensive study was initiated at ORNL to develop alloys based on the Ni-Mo binary system for the fuel-containing fluoride salt reactor where individual effects of Cr, Fe, Al, V, and Nb were investigated in detail [9]. This study initially led to the development of Hastelloy B (Ni-28% Mo-5% Fe) and Hastelloy W (Ni-25% Mo-5% Cr-5% Fe)[36]. The predominance of Ni and Mo in these alloys resulted in very good corrosion resistance in the molten fluoride salt, but these alloys exhibited embrittlement effects at higher Mo contents in the temperature range of 650 to 815 °C due to the formation of intermetallic phases. Another problem with these alloys was formation of a $NiMoO_4$ oxide layer on the air side that tended to spall during thermal cycling. The embrittlement problem was eliminated by reducing the Mo content to 15 to 17%. To provide air-side oxidation resistance, 6 to 8% Cr was added to the alloy. The result was alloy INOR-8 with a nominal composition of 15 to 17% Mo, 6 to 8% Cr, 4 to 6% Fe, and 0.04 to 0.08% C, and the balance of the composition was Ni. This alloy is also referred to as Alloy N and is commercialized as Hastelloy N [9,10,39]. The alloy is a single-phase solid solution, although randomly distributed carbide precipitates have been observed after elevated temperature exposure between 593 and 871 °C [39]. Corrosion weight change results for Hastelloy N in a fuel containing molten fluoride salt are shown in Figure 12.4.

A problem identified with Hastelloy N in the MSRE experiments was the development of cracks after exposures to molten fuel containing salt [11–13,36]. A detailed post-test examination of samples and subsequent separate effects tests showed the presence of fission product tellurium aggregated at the grain boundaries to be a prime cause of cracking. It has been noted that the presence of fission products with negative oxidation states can lead to the formation of brittle intergranular precipitates in metallic structural components [1]. Tellurium that exists in the salt as a metallic element can interact with the Cr and Ni in structural steels according to the reactions:

$$x\mathrm{Te} + y\mathrm{Ni} \rightarrow \mathrm{Ni}_y\mathrm{Te}_x \tag{12.26}$$

$$x\mathrm{Te} + y\mathrm{Cr} \rightarrow \mathrm{Cr}_y\mathrm{Te}_x \tag{12.27}$$

Because tellurium, along with elements that form higher valence fluorides, such as molybdenum, niobium, and ruthenium, forms a relatively unstable fluoride, it is likely to deposit onto metal surfaces to allow the aforementioned reactions to occur [12,13]. So while Hastelloy N was optimized for general corrosion resistance in salt, an intergranular attack by fission product tellurium was a concern.

Systematic experiments to investigate the detrimental effects of tellurium involved exposure of samples to tellurium vapor and testing alloys in molten salt with $Cr_3Te_4 + Cr_5Te_6$

additions [14,36]. In both cases, tellurium was observed at the grain boundaries of the alloy, and its diffusion depth into the alloy varied as the square root of exposure time. One approach found to be effective in reducing tellurium-induced stress corrosion cracking was to control the redox potential of the salt by controlling the U^{+4}/U^{+3} ratio as discussed earlier. It was shown that maintaining this ratio below 60 created reducing conditions that reduced cracking dramatically, as shown in Figure 12.12. The concept was based on controlling tellurium activity by complexing the tellurium with other metallic salt constituents, for example [11],

$$2UF_3 + MF_2 + xTe \leftrightarrow MTe_x + 2UF_4 \tag{12.28}$$

If the UF_3 to UF_4 ratio became too low, additions of beryllium metal could be used to remove some of the fluoride ions from the uranium [36]. Another approach to mitigate tellurium-induced cracking was to modify the composition of Hastelloy N by additions of 1 to 2% Nb, as shown in Figure 12.13.

Another issue observed in Hastelloy N was embrittlement and radiation hardening caused by helium produced by the transmutation of nickel atoms under radiation and the subsequent migration of helium to the grain boundaries. Additions of about 2% Ti reduced this effect dramatically by the formation of fine carbides, which acted as sites for helium, thereby preventing its migration to grain boundaries [5].

In most recent molten salt reactor concepts being proposed, such as the FHR, the release of fission products into the coolant would only happen if a fuel element fails and fission products are leached into the coolant [19–21]. Hastelloy N continues to receive consideration for use in future molten salt-cooled reactor concepts from the standpoint of its well-established corrosion resistance in high-temperature molten fluoride salts. However, more information and testing are required regarding the mechanical properties to qualify the alloy under Code Section Subsection NH of ASME boiler and Pressure Vessel Code (BPVC) for the high temperatures being targeted for the advanced molten salt-based reactor concepts [39].

Work conducted in Russia using the ORNL studies as a basis has led to the development of alloys with improved corrosion in molten fluoride fuel salts with and without the presence

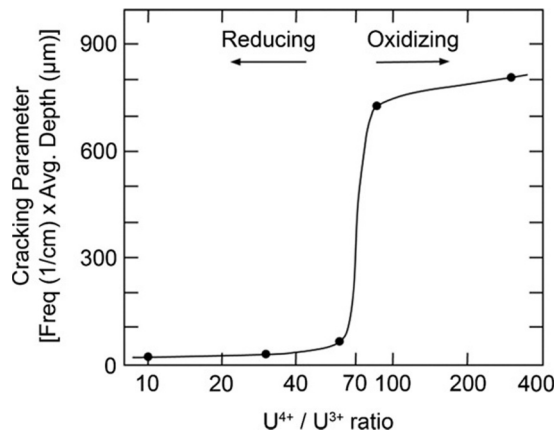

Figure 12.12 Intergranular cracking behavior of Hastelloy N specimens exposed to fuel bearing molten fluoride salt with additions of Cr_3Te_4 and Cr_5Te_6 at 700 °C [11].

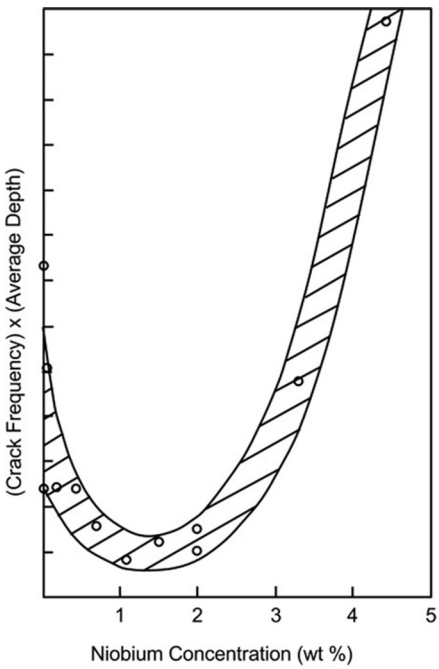

Figure 12.13 Modifying the composition of Hastelloy N by additions of 1 to 2% Nb reduced tellurium-induced cracking.

of radiation and applied stresses [36]. These include HN80MT (Ni-6.9% Cr-0.02% C-12.2% Mo-1.6% Ti- 2.6% Nb), HN80MTY (Ni-6.8% Cr-13.2% Mo-0.28% Fe-1.12% Al-0.072% W-0.04% Nb-0.02% C), and MONICR (Ni-6.85% Cr-15.8% Mo-2.27% Cr-0.13% Nb-0.16% Al-0.014% C). Alloying with Al at the expense of Ti revealed notable improvements in corrosion resistance and mechanical properties, and intergranular corrosion is reported to have reached a minimum value at an Al content of 2.6% Al.

Other alloys have also been investigated for corrosion in molten fluoride salt environments. The differences in experimental details, such as impurity levels in salt and test containers in various studies, often do not allow for a direct comparison of corrosion rates and depths, but certain general trends do emerge. When tested in molten LiF-BeF_2 (FLiBe) salt at 650 °C, 316 stainless steel showed a projected corrosion rate of 8 μm/year between 3000 and 9000 h of testing when tested in a 316 stainless-steel flow loop [6]. In the same experiment, the chromium content of the salt increased from 40 to 450 ppm in the first 3000 h of testing. However, in fuel-containing molten salt at 662 °C, the corrosion rate of 316 stainless steel was 25 μm/year due to the higher reactivity of the fuel salt [30]. Type 304 stainless steel tested in a 304 stainless-steel loop exposed to fuel salt (maximum temperatures between 668 and 685 °C) for 9.5 years showed a uniform corrosion rate of 22 μm/year, but voids extended into the matrix for about 250 μm [30]. In the same study, maraging steel (Fe-12Ni-5Cr-3Mo) showed a corrosion rate of only 14 μm/year, while for comparison, in these studies, Hastelloy-N showed a corrosion rate of 1.5 μm/year. In a more recent study, the corrosion rate of 304 and 316 stainless steels in molten LiF-BeF_2 (FLiBe) salt at 600 °C was estimated to be 10.6 and 5.4 μm/year, respectively, when tested in containers of the same material as the test materials [47]. Corrosion occurred by attack at the grain boundaries. Despite these moderately low corrosion rates, a reliable use of stainless steels in molten

fluoride salts will require continuous redox control with elements such as Be [6,35]. It should also be pointed out here that stainless steels and other iron-based materials did not show the grain boundary cracking observed in Hastelloy N when tested in fuel salts [12,14]. Corrosion of reduced activation steel (Fe-8.92% Cr-2 W) has been investigated in molten FLiNaK and FLiBe salts at 500 and 600 °C for exposures of 1000 h [48]. FLiBe tests performed in a crucible of the same steel (Fe-8.92% Cr-2 W) showed a corrosion depth of 0.637 μm in both 500 and 600 °C temperature tests. Corrosion in FLiNaK performed only at 600 °C showed a strong dependence of corrosion depth on the test container material. The depth of attack in molten FLiNaK salt when performed in a container made of the reduced activation steel was 6.73 μm, significantly higher than that observed for FLiBe salt under the same test conditions. The depth of attack in the reduced activation steel was about 24 μm when tested in a nickel container and there was a thickness gain of 0.084 μm observed on the steel samples when tested in a niobium container. This is again illustrative of the effect of dissimilar metal corrosion discussed earlier. Refractory metal compositions have also been investigated. The TZM (Mo-0.5% Ti-0.08Zr-0.02% C) alloy was tested in a LiF_2-BeF_2-ThF_4-UF_4 salt at temperatures as high as 1100 °C for 1000 h [15]. Leaching of Zr and Ti into the salt was observed, and the corrosion rate seemed to be related to the bulk diffusion of the corroding species to the surface of the alloy. Recrystallization was observed at the alloy surface and was attributed to the depletion of Ti and Zr, and the depth of removal of these elements was 20 and 100 μm, respectively. In molten CaF_2-MgF_2 molten salt at 930 °C W and Ta showed little corrosion, although the volatility of refractory metal fluorides in the open system will have to be considered [37,38].

Corrosion of yttria-stabilized zirconia has been tested in FLiNaK from700 to 900 °C for up to 360 h [49]. The corrosion depth was dependent on sintering parameters and grain size of the oxide. As may be expected, corrosion was quite severe, and depending on sintering conditions, the depths of attack were 150 and 400 μm at 800 and 900 °C, respectively. Corrosion rates of a number of materials in molten fluoride salts have been complied in the literature [9,34,36].

As discussed previously, high temperature alloys such as Hastelloy X, Haynes 230, and Incoloy 800H have been studied in molten FLiNaK salt at 850 °C using graphite containers [29,40,41]; however, the high chromium content of these alloys led to severe corrosion due to the dissolution of chromium. In further studies at the University of Wisconsin, stainless-steel containers were used to test the corrosion of 316 stainless steel and Hastelloy N samples separately in FLiNaK at 850 °C [50]. Additionally, tests were also performed with graphite test samples also immersed in salts with either 316 stainless steel or Hastelloy N samples. Weight change measurements summarized in Figure 12.14 show very limited corrosion compared to those observed in tests performed in graphite crucibles discussed earlier in this chapter (see Figure 12.5). The 316 stainless-steel test flats lost a miniscule amount of weight when tested in stainless-steel containers, as no dissimilar metals were involved. Figure 12.15 shows an EDS line scan depicting the affected depth in 316 stainless-steel samples with and without graphite coupons. As can be seen, the presence of graphite does promote the depletion of some chromium from the 316 stainless-steel surface. The outcomes with graphite present in the tests were particularly interesting in that a uniform chromium film was deposited on the graphite surface, which transformed to carbides (Figure 12.16). For the Hastelloy-N samples tested in the 316 stainless-steel containers (without graphite), a slight weight gain was observed due to the migration of chromium from higher chromium 316 stainless steel to the lower chromium Hastelloy N due to activity gradients.

Because Ni is relatively immune to the formation of fluorides, Ni electroplating has been investigated as a method for mitigating corrosion [29,51]. The weight loss measurements of Incoloy-800H, Ni-201, and Ni-plated Incoloy-800H after testing in molten FLiNaK salt at

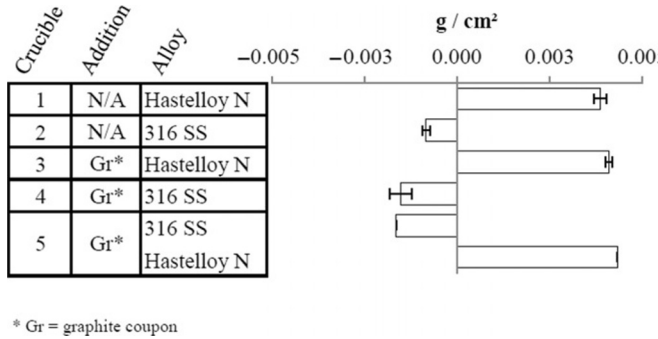

Figure 12.14 Weight change results of Hastelloy N and 316 stainless steel after testing in molten FLiNaK salt at 850 °C for 1000 h; Gr* represents the copresence of graphite with samples in the molten salt. Tests were performed in 316 stainless-steel containers [50].

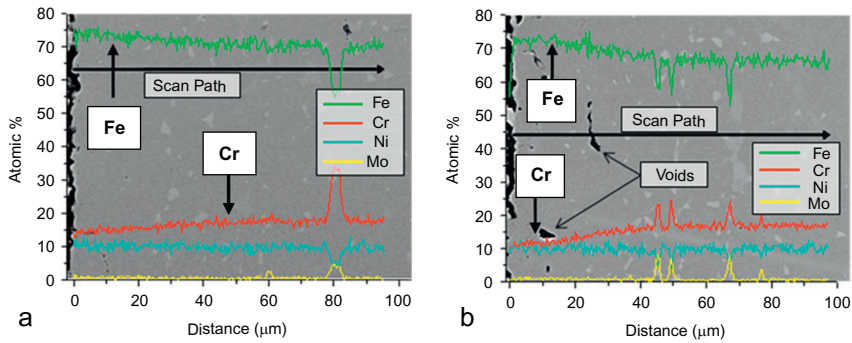

Figure 12.15 Cross-sectional SEM micrographs and corresponding EDS compositional line scan analysis of 316 L samples after testing in molten FLiNaK at 850 °C for 1000 h (a) without graphite and (b) with graphite. Tests were performed in 316 stainless-steel containers [50].

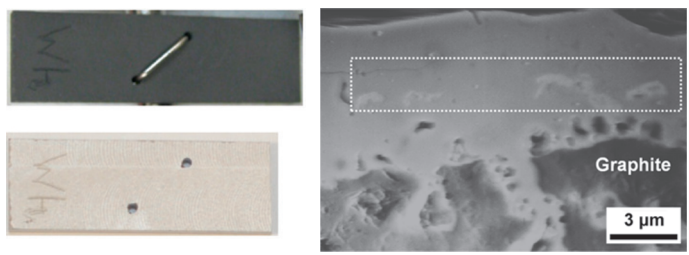

Figure 12.16 (a) Typical appearance of graphite samples prior to exposure (top) and after exposure to molten FLiNaK salt at 850 °C for 1000 h alongside 316 stainless-steel samples and (b) deposition of Cr on graphite coupon (phases in the dotted box are Cr_7C_3 and Mo_2C). Tests were performed in 316 stainless-steel containers [50].

850 °C for 500 h in graphite containers are shown in Figure 12.17. Ni plating reduced the corrosion of Incoloy-800H as measured by weight change dramatically, and the results are consistent with the measurements of chromium concentration in the salt after corrosion tests with each material (Table 12.2). Figure 12.18 shows the SEM cross-sectional image of the Ni-plated Incoloy 800H after these corrosion tests, along with the elemental EDS line scan confirming that chromium out diffusion into the salt is mitigated by Ni plating.

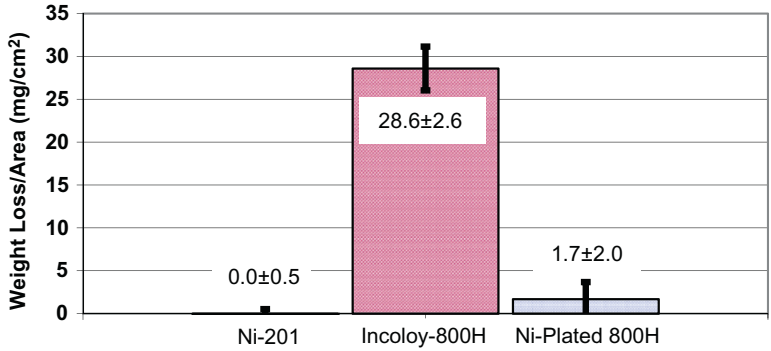

Figure 12.17 Average weight loss per area of Ni-201, Incoloy-800H, and Ni-plated Incoloy-800H coupons after exposure to molten FLiNaK at 850 °C for 500 h in graphite containers [29].

Table 12.2 Cr Content of FLiNaK Salt Before and After 850 °C, 500-h Corrosion Tests Performed in Graphite Containers [29][a]

Materials Exposed to FLiNaK Salt	Cr Content (Weight ppm)
As received FLiNaK	4.02 ± 0.49
Ni-201	3.59 ± 0.21
Ni-plated Incoloy-800H	77.29 ± 3.94
Incoloy-800H	371.85 ± 20.91

[a]Corrosion tests were performed in graphite containers, and salts were analyzed using neutron activation analysis.

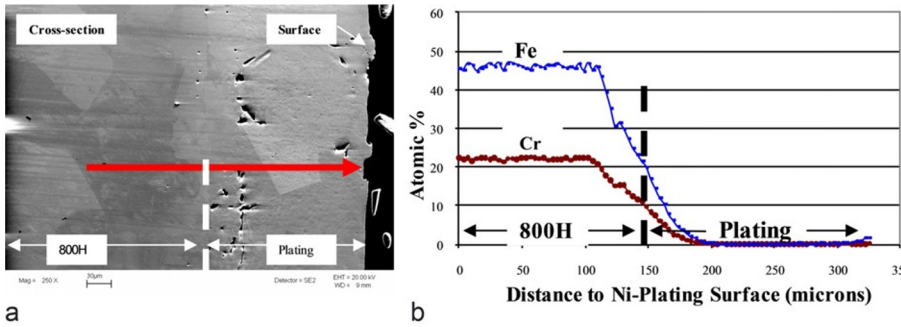

Figure 12.18 (a) Cross-sectional SEM image of Ni plating (≈175 μm) on Incoloy-800H after exposure to molten FLiNaK salt at 850 °C for 500 h and (b) corresponding EDS line scan for Fe and Cr [51].

12.3 Corrosion in Molten Chloride Salts

In the area of nuclear energy systems, molten chloride salts are being considered as heat transport fluids to transfer high-temperature process heat from nuclear reactors to power chemical plants [3,24,25]. Electrochemical reprocessing of used metallic fuel is performed routinely in molten LiCl-KCl electrolyte [23]. Molten NaCl-KCl-$MgCl_2$ salt was used in reprocessing of the liquid metal fuel (Bi + U + fission products) at Brookhaven National Laboratory (BNL) in the 1950s as part of the Liquid Metal Reactor Experiment (LMR). Molten chloride fueled salts are being considered for fast breeder reactors for *in situ* plutonium recycling [52].

Free energy of formation vs temperature diagrams (similar to Ellingham diagrams) constructed for chlorides show that alkali chlorides and alkaline earth chlorides are more thermodynamically favored than the transition metal chlorides [53]. It is then expected that the salt would not be reduced by common alloying elements, and no corrosion should occur when structural alloys are in contact with molten chloride salts. Thus, as in the case of molten fluoride salts, corrosion in molten chlorides is, to a great extent, driven by the impurities in the salt, typically H_2O, OH^-, O_2, and H^+ [52–63]. For example, the presence of moisture can lead to the formation of HCl with its attendant effects of corrosion.

Chloride ions can destabilize passive surface oxide films; however, the fluxing action is not as severe as fluoride salts. In chloride salts, the oxides are favored thermodynamically, although the ability to form a stable passivating oxide layer on the metal has been proven to be a much more difficult task than in oxidizing environments and aqueous solutions [42]. However, passivity has been observed in many alloys in molten salt potentiodynamic electrochemical tests. For example, in studies on the electrochemical behavior of iron, nickel, cobalt, copper, and molybdenum in molten LiCl-KCl eutectic salt containing lithium and oxygen ions at 375 and 400 °C, the current-potential curves exhibited characteristic corrosion–passivation behavior found in aqueous systems [54]. In studies performed on Ni in molten NaCl-KCl salt with small additions of sodium carbonate, it was observed that current density decreased with increasing the concentration of sodium carbonate [55]. O^{2-} ions from the carbonate passivated the surface and reduced the corrosion rate.

The corrosion mechanisms outlined for the corrosion of Ni-based superalloy Hastelloy X in the $NdCl_3$-NaCl-KCl mixture at 550, 600, and 800 °C is illustrative of several scenarios that can occur in molten chloride corrosion [52]. This study was performed for fast breeder reactors for *in situ* plutonium recycling with $NdCl_3$ being used as the surrogate for UCl_3 and $PuCl_3$. The native oxides on the alloy surface can react with $NdCl_3$ to form more stable neodymium oxychloride:

$$NiO + NdCl_3 = NiCl_2 + NdOCl \tag{12.29}$$

$$NiCr_2O_4 + NdCl_3 = NiCl_2 + Cr_2O_3 + NdOCl \tag{12.30}$$

$$NiFe_2O_4 + NdCl_3 = NiCl_2 + Fe_2O_3 + NdOCl \tag{12.31}$$

Residual moisture in chloride salts (chloride salts are quite hygroscopic) can react with $NdCl_3$ to form a neodymium oxychloride and corrosive HCl:

$$NdCl_3 + H_2O = NdOCl + 2HCl \tag{12.32}$$

Metals such as Mn, Cr, Fe, and Cu can get chlorinated by HCl at high temperatures:

$$M + xHCl = MCl_x + \frac{x}{2}H_2 \tag{12.33}$$

$$2FeCl_2 + 2HCl = Fe_2Cl_6(gas) + H_2 \tag{12.34}$$

As in the case of fluoride salts, moisture in the salt, even in small amounts, can enhance corrosion rates dramatically. For example, in this study, in the presence of some moisture, the corrosion rate increased by about an order of magnitude in the temperature range of 550 to 600 °C. Refractory metals, molybdenum and tungsten, were observed to be relatively immune to corrosion, as their chlorination by HCl generally does not occur until high temperatures due to Gibbs free energy considerations. The detrimental effects of trace amounts of moisture on the corrosion of Fe and Ni in molten NaCl-KCl salt has been demonstrated in electrochemical studies [54].

Some of the early corrosion studies in chloride salts were performed in relation to heat treatment baths. As an example, one such work examined the corrosion of four different Fe-Cr-Ni alloys in NaCl-KCl-$CaCl_2$-$BaCl_2$ molten salt [57]. It was determined that Cr is the most readily attacked element. It was also determined that, for alloys with similar chemical compositions, corrosion increased with increasing carbon content of the alloy. The addition of carbide-forming elements such as Nb and Ti reduced corrosion significantly. Studies at BNL under the LMFRE experiment on iron-based, nickel-based, refractory metals, and some ceramics in NaCl-KCl-$MgCl_2$ molten salt showed very little corrosion. From these previous experiments, it was found that the elements in an alloy are attacked preferentially based on their nobility. The more active an element, the more it will be corroded and removed from the alloy, thus the ranking for attack for common structural metals is Cr, Fe, and Ni. This is also borne out by the EMF series collated by for various pure metals in various chloride salts [53]. In more recent studies performed in LiCl molten salt at 650 °C with incorporations of lithium metal and lithium-oxide and lithium-nitride, Inconel 600 and 625 performed superiorly to 304 and 316 stainless steels, possibly due to their higher Ni content [58]. In tests performed in LiCl-KCl molten salt at 500 °C, the corrosion performance of Fe-2.25% Cr-1Mo alloy was determined to be outstanding [59]. As a testament to the higher stability of oxides in general in chloride salts vs fluoride salts, plasma-sprayed coatings of yttria-stabilized zirconia on 316 stainless-steel substrates exhibited good corrosion performance in molten LiCl-KCl pyroprocessing salt at 500 °C, although chlorination of SiO_2, TiO_2, Al_2O_3, and Fe_2O_3 impurities in the coating has been suggested as a concern [61].

Limited studies have been performed on corrosion in molten KCl-$MgCl_2$ eutectic salt [53]. This salt has been identified as one of the lead candidate as a secondary heat transfer coolant in nuclear energy systems. A wide range of high-temperature Ni-based alloys, including Hastelloy X, Hastelloy N, Inconel 800H, Inconel 718, Inconel 625, Inconel 600, and Inconel 617, as well as Ni-201 and 316 stainless steel, were tested in this salt at 850 °C for 100 h in a quartz container. A corrosion attack for most of these alloys occurred almost exclusively along the grain boundaries and was accompanied by chromium dissolution into the molten salt. Hastelloy N exhibited the least grain boundary attack. In general, these studies showed that high Ni alloys were less resistant to corrosion attack than in FLiNaK fluoride salt, possibly due to the more ready formation of Ni-chloride that dissolves into the salt. A preferential attack of Cr was observed in almost all materials tested. However, the excessive attack observed in all the alloys may be due to the reaction between SiO_2 (from the quartz containers) and the KCl-$MgCl_2$ salt producing greater oxidizing conditions for the alloys. Figure 12.19 shows some typical cross-sectional images of the various alloys after corrosion testing in molten KCl-$MgCl_2$ salt after 100 h of testing. Data on corrosion attack in chloride salt are quite scant compared to fluoride salts, but when extrapolated to a yearly corrosion rate, data are typically several hundred micrometers to millimeters in thickness [34]. Clearly, both impurities and crucible material likely played a significant role in accelerating corrosion.

Studies performed at ORNL flow loops in LiCl-KCl and NaCl-KCl-$MgCl_2$ salt with maximum loop temperatures in the range of 500 and 575 °C for 347 and 410 stainless steel and

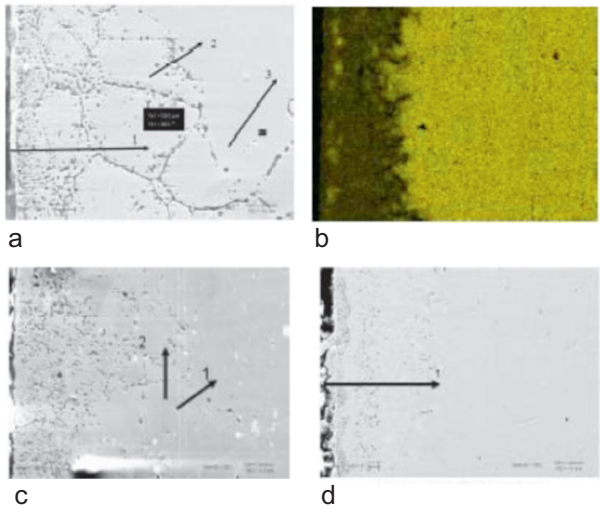

Figure 12.19 SEM cross-sectional images showing corrosion in various alloys after testing in KCl-$MgCl_2$ molten salt at 850 °C for 100 h in quartz crucible: (a) Inconel 617, (b) elemental X-ray mapping for Cr showing its depletion in Inconel 625, (c) Haynes 230, and (d) Inconel 718 [53].

2.25Cr-1Mo alloy also showed very high corrosion rates [24]. It is speculated that the results of all these studies were affected strongly by impurities emanating from the containment system or the environment, which attacked the protective oxide layer and exposed the alloy to dissolution. The effect of the cover environment is also critical in dictating corrosion. In a study on low carbon steels at 900 °C in molten KCl, it was noted that the corrosion rate increased by a factor of 4 when tested in air compared to argon and by a factor of 10 when performed in a HCl environment [62].

It is abundantly clear that reducing the impurity levels is imperative to reducing the corrosion of materials in molten chloride salts. Moisture in particular is an issue, as chloride salts tend to be hygroscopic. Furthermore, unlike fluoride salts where fluorination is quite effective in removing oxygen, chlorination is not quite as effective. Purification is typically achieved by a series of treatments starting with vacuum drying of the salt to remove moisture, followed by an extended dry HCl sparge, and finally an argon inert gas sparge to remove excess HCl. Sparging with carbon-tetrachloride may be an effective alternative to HCl sparging [53]. Contact with an active metal such as Mg can also be very effective in keeping impurities such as Fe and Ni to a minimum [34,53]. Treatments with ammonium chloride have also been recommended [34]. In LiCl salts, for example, the addition of Li metal was effective in lowering the redox potential of the salt and mitigated the corrosion of the test coupons [60]. Once purified, the salts must be stored in an evacuated environment and handled in atmosphere-controlled glove boxes.

12.4 Corrosion in Molten Fluoroborate Salts

Fluoroborate salts such as 8% NaF-92% $NaBF_4$ and 25% KF-75% KBF_4 (mol%) have been considered and tested as a candidate intermediate coolant salt and for tritium sequestration in the ORNL experiments [5]. The salt was tested in Inconel 600 convection loops for 11,500 h without excessive corrosion or visible attack on the impeller. Corrosion was sensitive to the presence of impurities, particularly moisture, which can lead to several tens of micrometers per year of corrosion damage. With reasonable impurity control, a corrosion rate of

18 μm/year has been obtained and, with stringent impurity, control corrosion rates could be reduced to 5 μm/year. In the presence of impurities, NaCr3F6 was deposited on the relatively cooler sections of the loop.

Typical culprit impurities in fluoroborate salts are the same as for fluoride and chloride salts, namely, moisture, air, or oxides emanating from the environment, the salt, or the containment materials. Speculated impurity-driven corrosion reactions include [16,36]

$$H_2O + NaBF_4 = NaBF_3OH + HF \tag{12.35}$$

$$NaBF_3OH = NaBF_2O + HF \tag{12.36}$$

$$6HF + 6NaF + 2Cr = 2Na_3CrF_6 + 3H_2 \tag{12.37}$$

Additionally, boron-trifluoride gas can be potentially generated, and its hydrolysis can lead to the production of highly corrosive HF gas. The purification approaches for fluoroborate salts are less well established, and treatment with BF_3 and HF gases has been attempeted with limited success [36].

12.5 Radiolysis Effects on Corrosion

Previous work and literature indicate that molten fluoride salts are radiolytically stable; consequently, the effect of radiolysis on corrosion is not expected to be significant [33,34,36]. No detectable degradation of the salts was observed in ARE and MSRE programs, and the salts were resistant to reactor radiation, uranium fissions in the salt, and accumulation of fission products. While radiation will dissociate fluorides, the recombination effects are kinetically dominant in molten salts and no F_2 is released from the salt [34]. In theory, however, transmutation of Li and F can generate H and O, which could result in the formation of H_2O, O_2, and H_2 and could increase the oxidation potential of the salt. The neutron cross section of salt constituents must be low enough to avoid an excessive parasitic capture of neutrons. A compilation of neutron cross sections of common salt constituents shows that they have low neutron cross sections [33]. For example, ^{7}LiF, BeF_2, RbF, and MgF_2 have thermal capture cross sections of 0.033, 0.01, 0.70, and 0.63 barns, respectively. Chloride salts, however, have not been considered for primary coolants because of the need for isotopic separation of chlorine to avoid high cross-section nuclides and waste management challenges associated with the activation product ^{36}Cl [33,34,36].

12.6 Conclusions

Molten salts have a long history of use in nuclear energy systems as fuel-bearing primary coolants, secondary intermediate heat exchange coolants for heat transfer, and fuel recycling. Corrosion of construction materials for these systems for uninterrupted long-term use continues to be an important consideration. In fluoride salts, which perhaps have the longest history of experience, the protective oxide layer on alloys typically relied upon for high-temperature corrosion resistance dissolves, thereby exposing the fresh alloy surface to the molten salt. In molten chloride salts, passivity has been observed; however, the oxide layer is prone to attack and may not provide the necessary corrosion protection. In both cases, the constituents of the salt cannot be reduced thermodynamically by common structural alloys.

However, impurities present in the salt can result in a significant corrosion attack. These impurities can emanate during the preparation and storage of the salt, either from the environment or containment materials, and react with the oxide impurities on the system walls. Minimizing impurities is crucial to corrosion control and many procedures have been developed to curtail impurities, but further research is required in this area. Corrosion can be enhanced further by the presence of dissimilar metals due to activity-driven corrosion. This issue must be considered when multiple materials are present in the vicinity of each other in the molten salt. Mass transfer of corrosion products from hotter sections of the system and their subsequent deposition on the relatively cooler sections can be a problem and can clog heat exchanger systems. Given that corrosion will occur, techniques to implement redox control must be implemented and the salt chemistry must be monitored constantly. Development of new alloys, possibly combined with surface treatments, with higher thermodynamic resistance to corrosion in molten salts, must be pursued.

References

[1] Delpech, S., Cabet, C., Slim, C., Picard, G.S. (2010). Molten fluorides for nuclear applications. *Mater. Today*, **13**(12), 34–41.

[2] Calderoni, P., Sharpe, P., Nishimura, H., Terai, T. (2009). Control of molten salt corrosion of fusion structural materials by metallic beryllium. *J. Nucl. Mater.*, **386–388**, 1102–1106.

[3] Williams, D.F., Clarno, K.T. (2008). Evaluation of salt coolants for reactor applications. *Nucl. Technol.*, **163**, 330–343.

[4] Rosenthal, M.W., Kasten, P.R., Briggs, R.B. (1970). Molten salt reactors: History, status, and potential. *Nucl. Technol.*, **82**, 111–122.

[5] MacPherson, H.G. (1972). Development of materials and systems for molten salt-reactor concept. *Reactor Technol.*, **15**(2), 136–155.

[6] Keiser, J.R., DeVan, J.H., Lawrence, E.J. (1979). Compatibility of molten salts with type 316 stainless steel. *J. Nucl. Mater.*, **85/86**, 295–298.

[7] Grimes, W.R. (1970). Molten salt reactor chemistry. *Nucl. Appl. Technol.*, **8**, 137–155.

[8] Perry, A.M. (1967). Physics Program for Molten Salt Breeder Reactors. ORNL-TM-1851 & ORNL-TM-1857, Oak Ridge National Laboratory, Oak Ridge, TN.

[9] DeVan, J.H. (1969). Effect of Alloying Additions on Corrosion Behavior of Ni-Mo Alloys in Fused Fluoride Mixtures. ORNL-TM-2021, Oak Ridge National Laboratory, Oak Ridge, TN.

[10] Alloy Compatibility with LiF-BeF_2 Salts Containing ThF_4 and UF_4. ORNL-TM-4286, Oak Ridge National Laboratory, Oak Ridge, TN.

[11] Keiser, J.R. (1977). Status of Tellurium-Hastelloy N Studies in Molten Fluoride Salts. ORNL-TM-6002; Oak Ridge National Laboratory, Oak Ridge, TN.

[12] McCoy, H.E., McNabb, B. (1972). Intergranular Cracking of INOR-8 in the MSRE. ORNL-TM-4829; Oak Ridge National Laboratory, Oak Ridge, TN.

[13] Grimes, R.B. (1967). Summary of the Objectives, the Design, and a Program Development of Molten Salt Breeder Reactors. ORNL-TM-1851; Oak Ridge National Laboratory, Oak Ridge, TN.

[14] McCoy, H.E. (1978). Status of Materials Development for Molten Salt Reactors. ORNL-TM-5920; Oak Ridge National Laboratory, Oak Ridge, TN.

[15] Koger, J.W., Litman, A.F. (1969). Compatibility of Molybdenum-Base Alloy TZM with LiF-BeF_2-ThF_4-UF_4 at 1100 °C. ORNL-TM-2724; Oak Ridge National Laboratory, Oak Ridge, TN.

[16] Bamberger, C.E., Baes, C.F. (1973). Corrosion of Hastelloy N by Fluoroborate Melts. ORNL-4832; Oak Ridge National Laboratory, Oak Ridge, TN.

[17] Koger, J.W. (1972). Effect of FeF_2 Addition on Mass Transfer in a Hastelloy N–LiF-BeF_2-UF_4 Thermal Convection Loop. ORNL-TM-4188; Oak Ridge National Laboratory, Oak Ridge, TN.

[18] Evaluation of Hastelloy N Alloys after Nine Years Exposure to Both Molten Fluoride Salt and Air at Temperatures from 700 °C to 560 °C. ORNL-TM-4189; Oak Ridge National Laboratory, Oak Ridge, TN.

[19] Forsberg, C.W., Peterson, P.F., Kochdarfer, R.A. (2008). Design Options for the Advanced High-Temperature Reactor. *Proc. ICAPP '08*; Anaheim, CA, June 8-12, Paper 8026.
[20] Holcomb, D.E., Setiner, S.M., Flanagan, G.F., Peretz, F.J., Yoder, G.L. (2009). An Analysis of Testing Requirements for Fluoride Salt-Cooled High Temperature Reactor. ORNL/TM-2009/297; Oak Ridge National Laboratory, Oak Ridge, TN.
[21] Forsberg, C.W., Pickard, P., Peterson, P.F. (2003). Molten salt-cooled advanced high temperature reactor for production of hydrogen and electricity. *Nucl. Technol.*, **144**, 289–302.
[22] Ackerman, J.W., Johnson, T.R., Chow, L.S.H., Carls, E.L., Hannum, W.H., Laidler, J.J. (1997). Treatment of wastes in the IFR fuel cycle. *Prog. Nucl. Energ.*, **31**, 141–154.
[23] Inoue, T., Koch, L. (2008). Development of pyro-processing and its future directions. *Nucl. Eng. Technol.*, **40**, 183–190.
[24] Williams, D.F., Toth, L.M., Clarno, K.T. (2006). Assessment of Candidate Molten Salt Coolants for NGNP/NHI Heat Transfer Loop. ORNL/TM-2006/69; Oak Ridge National Laboratory, Oak Ridge, TN, USA.
[25] Davis, C.B. (2005). Implementation of Molten Salt Properties into RELAP5-3D/ATHENA. INEEL/EXT-05-02658; Idaho National Engineering and Environmental Laboratory, Idaho Falls, ID.
[26] Olson, L.C., Ambrosek, J.W., Kuwahara, N., Anderson, M.H., Sridharan, K., Allen, T.R. (2010). High Temperature Molten Salt as Heat Transfer Fluids: Corrosion and Flow Loop Studies. *Proc. Conf. High Temperature Reactor,* Prague, Czech Republic, October 18-20, Paper 61.
[27] Khanna, A.S. (2002). Introduction to High Temperature Oxidation and Corrosion. American Society for Materials International, ISBN 0-87170-762-4.
[28] Williams, D., Toth, L., Clarno, K., Forsberg, C.W. (2005). Assessment of Properties of Candidate Liquid Salt Coolants for the Advanced High Temperature Reactor (AHTR). ORNL/GEN4/LTR-05-001; Oak Ridge National Laboratory, Oak Ridge, TN.
[29] Olson, L.C. (2009). Materials Corrosion in Molten LiF-NaF-KF Eutectic Salt. Doctoral Thesis University of Wisconsin, Madison, WI.
[30] Koger, J.W. (1987). Fundamentals of high-temperature corrosion in molten salts. ASM Metals Handbook, Vol. 13, ASM International pp 50–55.
[31] Wilson, D. (2006). Corrosion Issues in Molten Fluoride Salts. *Proc. American Nuclear Society Annual Conference* Reno, NV.
[32] Williams, D., Wilson, D., Keiser, J., Toth, L., Caja, J. (2003). Research on Molten Fluorides as High Temperature Heat Transfer Agents. *Global 2003, Session 2A: Coolant/Material Interactions in Advanced Reactor Systems, Embedded Topical Within 2003 American Nuclear Society Winter Meeting*; pp 1–12.
[33] Forsberg, C.W. (2004). Reactors with Molten Salts: Options and Missions. In: *Frédéric Joliot & Otto Han Summer School on Nuclear Reactors, Physics, Fuels, and Systems;* Cadarache, France.
[34] Sohal, M.S., Ebner, M.A., Sabharwall, P., Sharpe, P. (2010). Engineering Database of Liquid Salt Thermophysical and Thermochemical Properties. INL/EXT-10-18297; Idaho National Laboratory, Idaho Falls, ID.
[35] Williams, D.F., Toth, L.M. (2005). Chemical Considerations for the Selection of the Coolant for the Advanced High Temperature Reactor. ORNL/GEN4/LTR-05-001Oak Ridge National Laboratory, Oak Ridge, TN.
[36] Ignatiev, V., Surenkov, A. (2012). Material performance in molten salts. In: R.J.M. Konings, *Comprehensive Nuclear Materials*, Vol. 5, Elsevier pp 221–250.
[37] Misra, A., Wittenberger, J. (1987). Fluoride Salts and Container Materials for Thermal Storage Applications in Temperature Range 973 to 1400 K. NASA-Lewis Technical Memorandum 89913.
[38] Whittenberger, J.D., Misra, A.K. (1987). Identification of Salt-Alloy Combinations for Thermal Energy Storage Applications in Advanced Solar Dynamic Power Systems. *J. Mater. Eng.*, **9**(3), 293–302.
[39] Ren, W., Muralidharan, G., Wilson, D.F., Holcomb, D.E. (2011). Considerations of Alloy N for Fluoride Salt-Cooled High-Temperature Reactor Applications. *Proc. ASME Pressure Vessels & Piping Division Conference* Baltimore, MD.

[40] Olson, L.C., Ambrosek, J.W., Sridharan, K., Anderson, M.H., Allen, T.R. (2009). Materials corrosion in molten salt LiF-NaF-KF salt. *J. Fluorine Chem.*, **130**, 67–73.
[41] Olson, L.C., Sridharan, K., Anderson, M.H., Allen, T.R. (2010). Intergranular corrosion of high temperature alloys in molten fluoride salts. *Mater. High Temp.*, **27**, 145–149.
[42] Edeleanu, C., Littlewood, R. (1960). Thermodynamics of corrosion in fused chlorides. *Electrochim. Acta*, **3**, 195–207.
[43] Littlewood, R., Argent, E.J. (1961). The effect of aqueous contaminants on the redox potential of chloride melts. *Electrochim. Acta*, **4**, 114–128.
[44] Del Cul, G.D., Williams, D.F., Toth, L.M. Redox Potential of Novel Electrochemical Buffers Useful for Corrosion Prevention in Molten Fluorides. http://www.ornl.gov/webworks/cppr/y2001/pres/112728.pdf.
[45] Olander, D. (2012). Redox potential in molten fluoride salts: Definition and control. *J. Nucl. Mater.*, **300**, 270–272.
[46] Ludwig, D., Olson, L.C., Sridharan, K., Anderson, M.H., Allen, T.R. (2011). High temperature electrochemistry of molten fluoride salt for measurement of dissolved chromium. *Corrosion Eng. Sci. Technol.*, **46**, 360–364.
[47] Kondo, M., Nagasaka, T., Sagara, A. (2009). Metallugical study on corrosion of austenitic steels in molten salt LiF-BeF_2 (FLiBe). *J. Nucl. Mater.*, **386–388**, 685–688.
[48] Kondo, M., Nagasaka, T., Xu, Q., Muroga, T., Sagara, A., Noda, N., Ninomiya, D., Nagura, M., Suzuki, A., Terai, T., Fujii, N. (2009). Corrosion characteristics of reduced activation ferritic steel, JLF-1 (8.92Cr-2 W) in molten salts FLiBe and FliNaK. *Fusion Eng. Des.*, **84**, 1081–1085.
[49] Stournaras, C.J., Tsetsekou, A., Zambetakis, T.H., Kontoyannis, C.G., Carountzos, G. (1995). Corrosion of yttria-fully stabilized zirconias in molten fluorides. *J. Mater. Sci.*, **30**, 4375–4379.
[50] Sellers, S. (2012). M.S. Thesis, University of Wisconsin, Madison, WI.
[51] Olson, L.C., Sridharan, K., Anderson, M.H., Allen, T.R. (2011). Nickel-plating for active metal dissolution resistance in molten fluoride salts. *J. Nucl. Mater.*, **411**, 51–59.
[52] Hosoya, Y., Terai, T., Yoneoka, T., Tanaka, S. (1997). Compatibility of structural materials with molten chloride mixture at high temperature. *J. Nucl. Mater.*, **248**, 348–353.
[53] Ambrosek, J.W. (2011). Molten Chloride Salts for Heat Transfer in Nuclear Systems. Ph.D. Thesis University of Wisconsin, Madison, WI.
[54] Feng, X.K., Melendres, C.A. (1982). Anodic corrosion and passivation behavior of some metals in molten LiCl-KCl containing oxide ions. *J. Electrochem. Soc.*, **129**, 1245–1249.
[55] Nishikata, A., Numata, H., Tsaru, T. (1991). Electrochemistry of molten salt corrosion. *Mater. Sci. Eng.*, **A146**, 15–31.
[56] Kochergin, V.P., Khaibullina, L.G., Potapova, O.G. (1956). Solubility of iron in fused zinc, alkali metal, and alkaline-earth metal chlorides. *J. Inorg. Chem. USSR*, **1**, 191–196.
[57] Jackson, J.H., LaChance, M.H. (1954). Resistance of cast Fe-Ni-Cr Alloys to corrosion in molten neutral heat treating salts. *Trans. ASM*, **46**, 157–183.
[58] Indacochea, J.E., Smith, J.L., Litko, K.R., Karell, E.J., Rarez, A. (2001). High temperature oxidation and corrosion of structural materials in molten chloride salts. *Oxid. Met.*, **55**, 1–16.
[59] Westphal, B.R., Li, S.X., Fredrickson, G.L., Vaden, D., Johnson, T.A., Wass, J.C. (2011). Evaluation of 2.25-1Mo Alloy for Containment of LiCl/KCl Eutectic during the Pyroprocessing of Used Nuclear Fuel. INL/CON-10-19580; Idaho National Laboratory, Idaho Falls, ID.
[60] Indacochea, J.E., Smith, J.L., Litko, K.R., Karell, E.J. (1999). Corrosion performance of ferrous and refractory metals in molten salts under reducing conditions. *J. Mater. Res.*, **14**, 1990–1995.
[61] Ravi Shankar, A., Mudali, U.K., Sole, R., Khatak, H.S., Raj, B. (2008). Plasma sprayed yttria-stabilized zirconia coatings on type 316 stainless steel for pyrochemical reprocessing plant. *J. Nucl. Mater.*, **372**, 226–232.
[62] Ozeryanaya, I.N. (1985). Corrosion of metals by molten salts in heat treatment processes. *Met. Sci. Heat Treat.*, **27**, 184–188.
[63] Johnson, T.R., Teats, F.G., Pierce, R.D. (1969). A Method for the Purification of Molten Chloride Salts. Technical Report ANL-7603; Argonne National Laboratory, Argonne, IL.